Supplementary Materials

"Future projections of the Greenland ice sheet energy balance driving the surface melt"

B. Franco, X. Fettweis, and M. Erpicum

***The Cryosphere*, 2012**

Table. S1. Relative anomalies (%) of the 2080-2099 NET energy flux and SEB components compared to the 1980-1999 results, on 1980-1999 MSK_{melt}, for the different future MAR runs performed in this study.

	NET	**SW_{net}**	**LW_{net}**	**SHF**	**LHF**
MAR-CAN$_{45}$	143.60	23.85	-6.05	86.22	-68.78
MAR-CAN$_{85}$	313.48	42.94	-18.67	211.79	-198.37
MAR-NOR$_{26}$	72.01	10.85	-2.01	39.89	-8.95
MAR-NOR$_{45}$	91.70	13.32	-3.52	46.42	-17.55
MAR-NOR$_{60}$	127.02	16.45	-6.98	60.42	-42.42
MAR-NOR$_{85}$	205.45	22.25	-14.64	104.52	-85.46
MAR-MIR$_{45}$	81.39	13.68	-5.24	29.44	-31.94
MAR-MIR$_{85}$	225.14	32.22	-14.12	118.93	-108.94

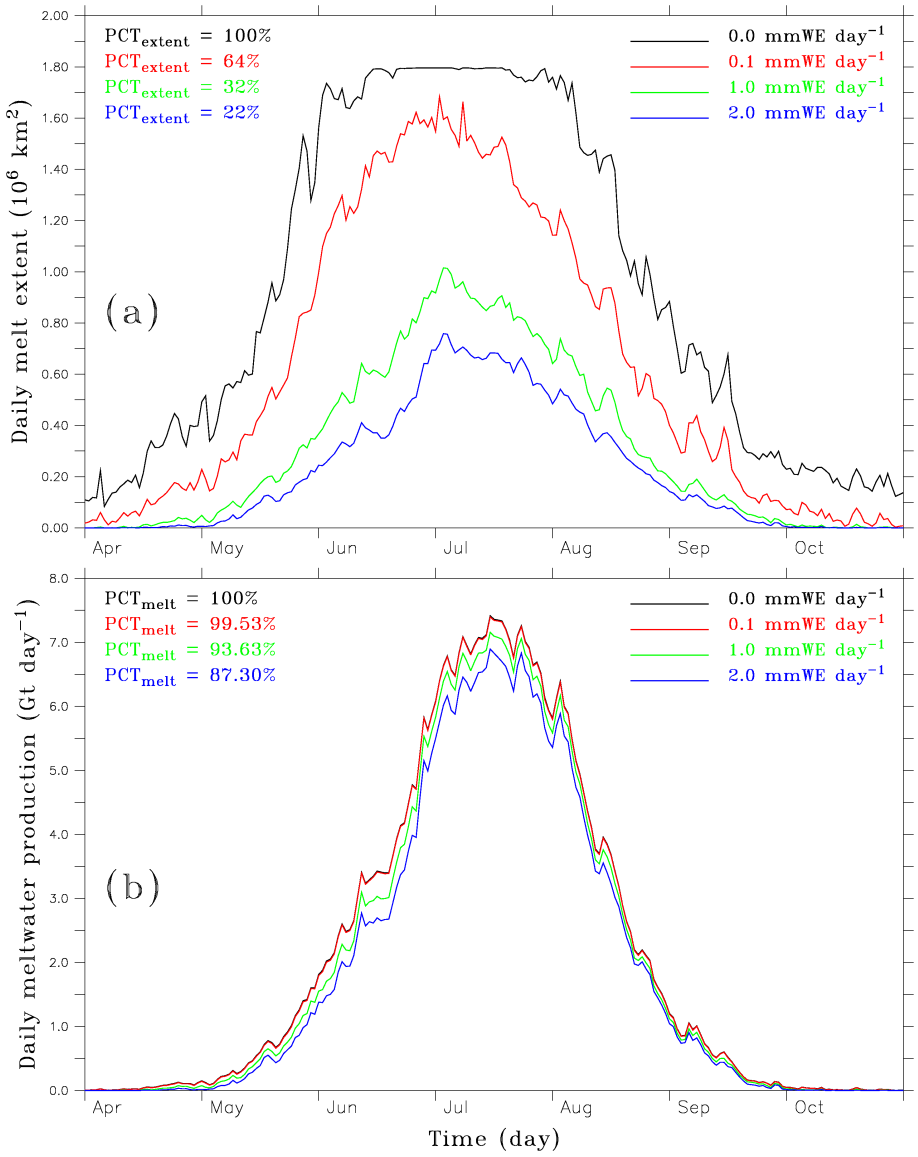

Fig. S1. (a) Daily melt extent (10^6 km^2) over the GrIS simulated by ERA-Interim-forced MAR over the 1980-1999 period, for different daily melt thresholds. PCT$_{extent}$ indicates the percentage of the annually-cumulated melt extent resolved for a given melt threshold. **(b)** The same as **(a)**, but for the daily meltwater production (Gt day^{-1}). PCT$_{melt}$ indicates the percentage of the annually-cumulated meltwater production resolved for a given melt threshold.

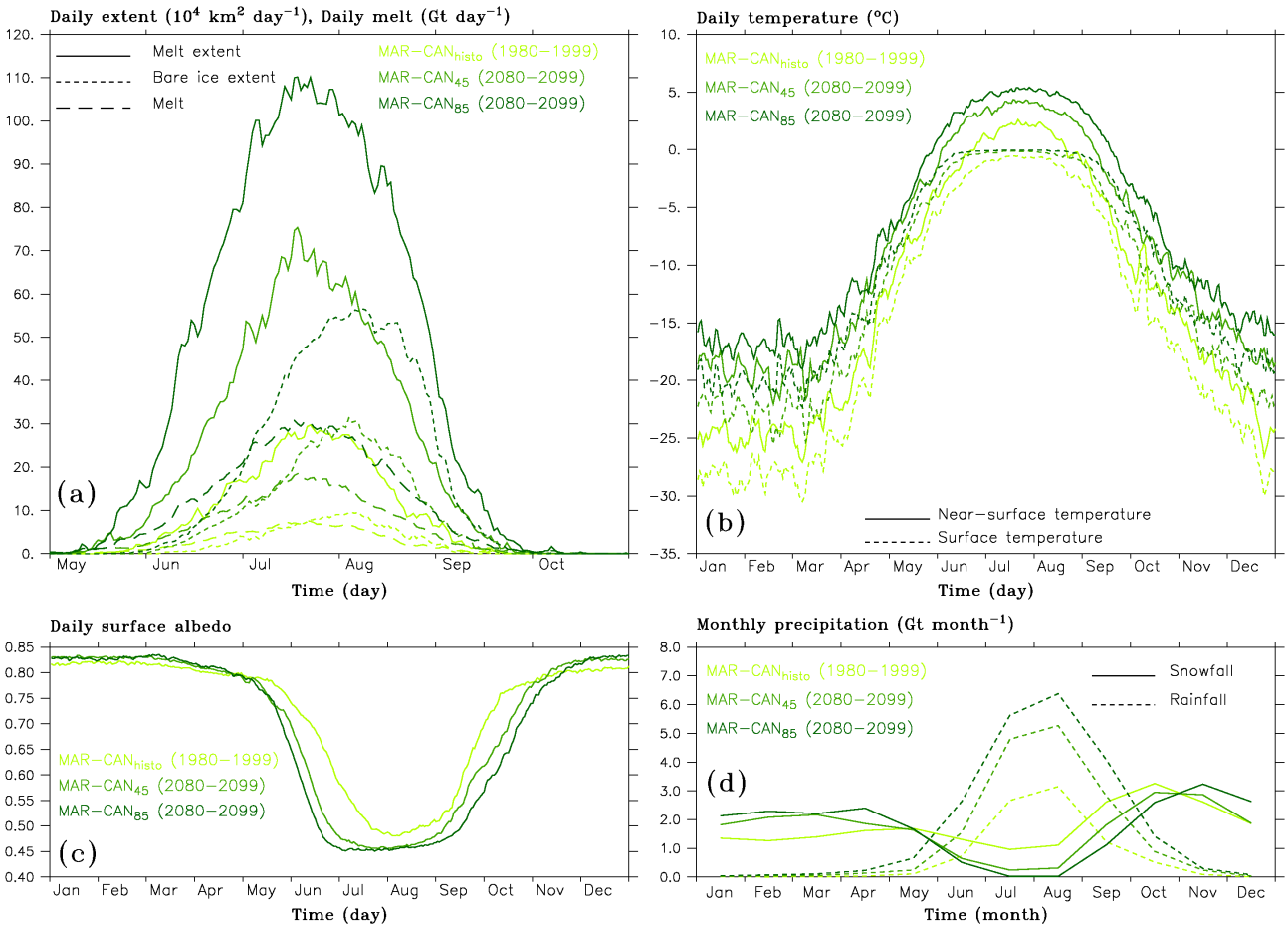

Fig. S2. (a) Daily melt and bare ice extents (10^4 km^2 day^{-1}) on the GrIS based on daily melting rate higher than 7.5 mmWE day^{-1}, and daily melt (Gt day^{-1}) from the 1980-1999 MAR-CAN$_{histo}$, 2080-2099 MAR-CAN$_{45}$ and MAR-CAN$_{85}$ simulations. **(b)** Daily near-surface (TAS) and surface (STT) temperatures (°C) from the same MAR simulations, on the maximum bare ice extent of the 1980-1999 MAR-CAN$_{histo}$ simulation. **(c)** The same as **(b)**, but for the daily surface albedo. **(d)** The same as **(b)**, but for the monthly snowfall (SF) and rainfall (RF) (Gt month^{-1}).

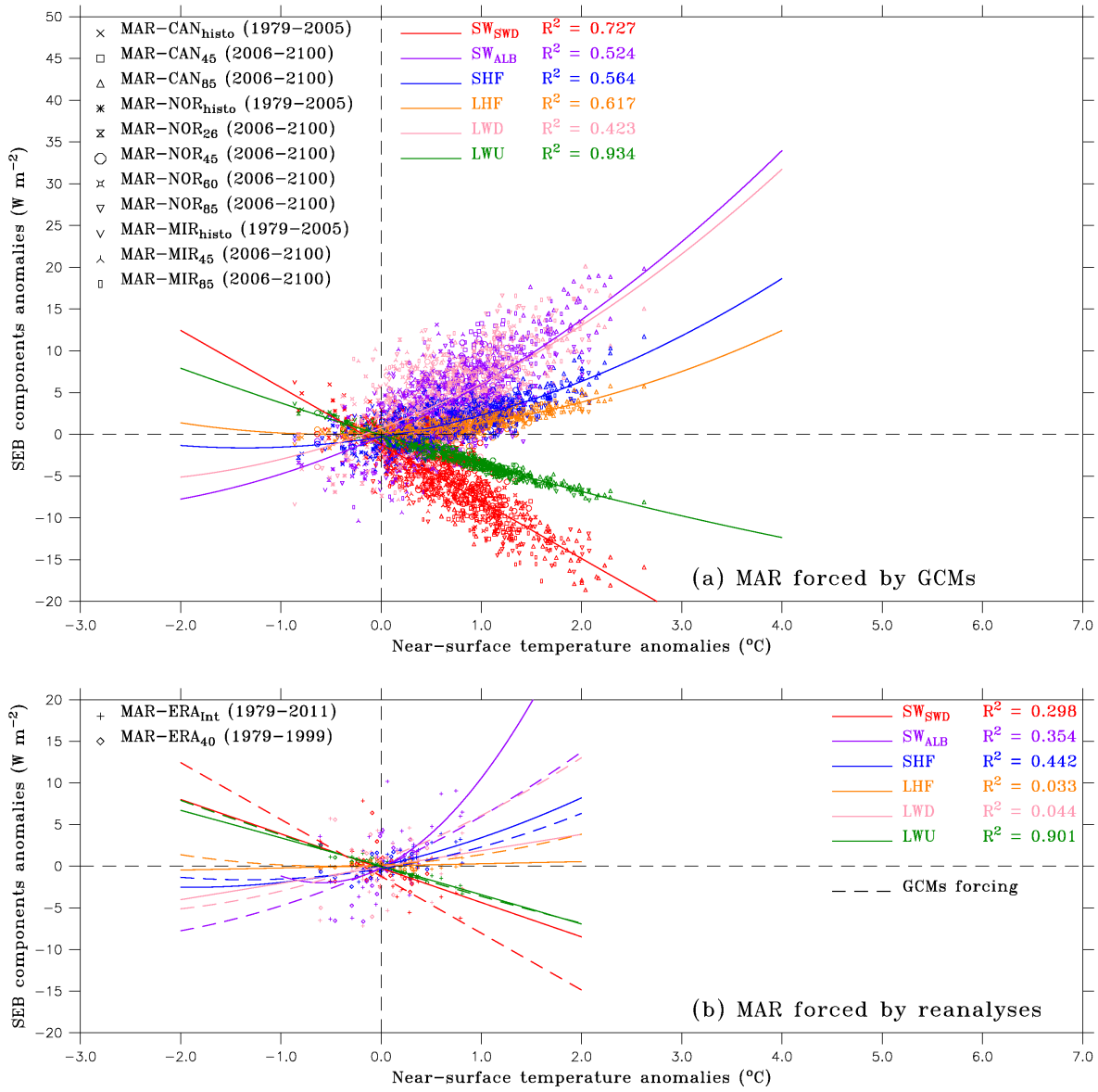

Fig. S3. (a) SEB components anomalies (W m^{-2}) from the GrIS according to the near-surface air temperature anomalies (°C) for the MAR simulations forced by CMIP5 GCMs, with regressions drawn in solid lines. All the anomalies are related to the 1980-1999 average outputs provided by MAR forced with the same forcing fields. For a given year of simulation, the daily SEB components and near-surface air temperatures where a daily melt greater than 1 mmWE day^{-1} occurs have been annually averaged on the GrIS according to the occurrence of the daily melt events. **(b)** The same as **(a)**, but for the MAR simulations forced by the ERA-Interim and ERA-40 reanalyses, with the regressions from **(a)** drawn in dashed lines.

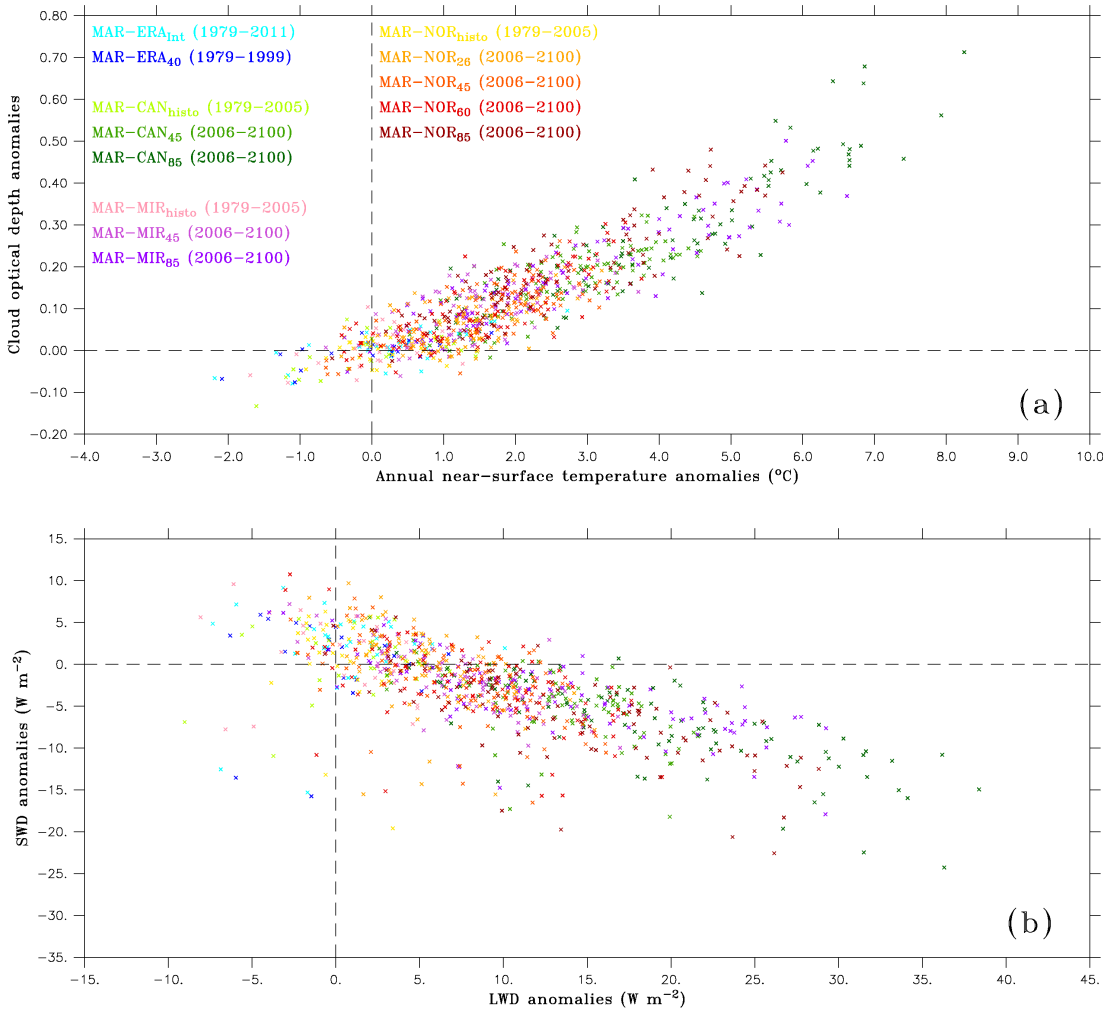

Fig. S4. (a) Annual cloud optical depth (COD) anomalies over the GrIS according to the annual near-surface air temperature anomalies (°C), for the MAR simulations forced by the reanalyses and the CMIP5 GCMs. All the annual anomalies are related to the 1980-1999 average outputs provided by MAR forced with the same forcing fields. **(b)** The same as **(a)**, but for the annual shortwave downward flux (SWD) anomalies (W m^{-2}) according to the annual longwave downward flux (LWD) anomalies (W m^{-2}) over the GrIS.

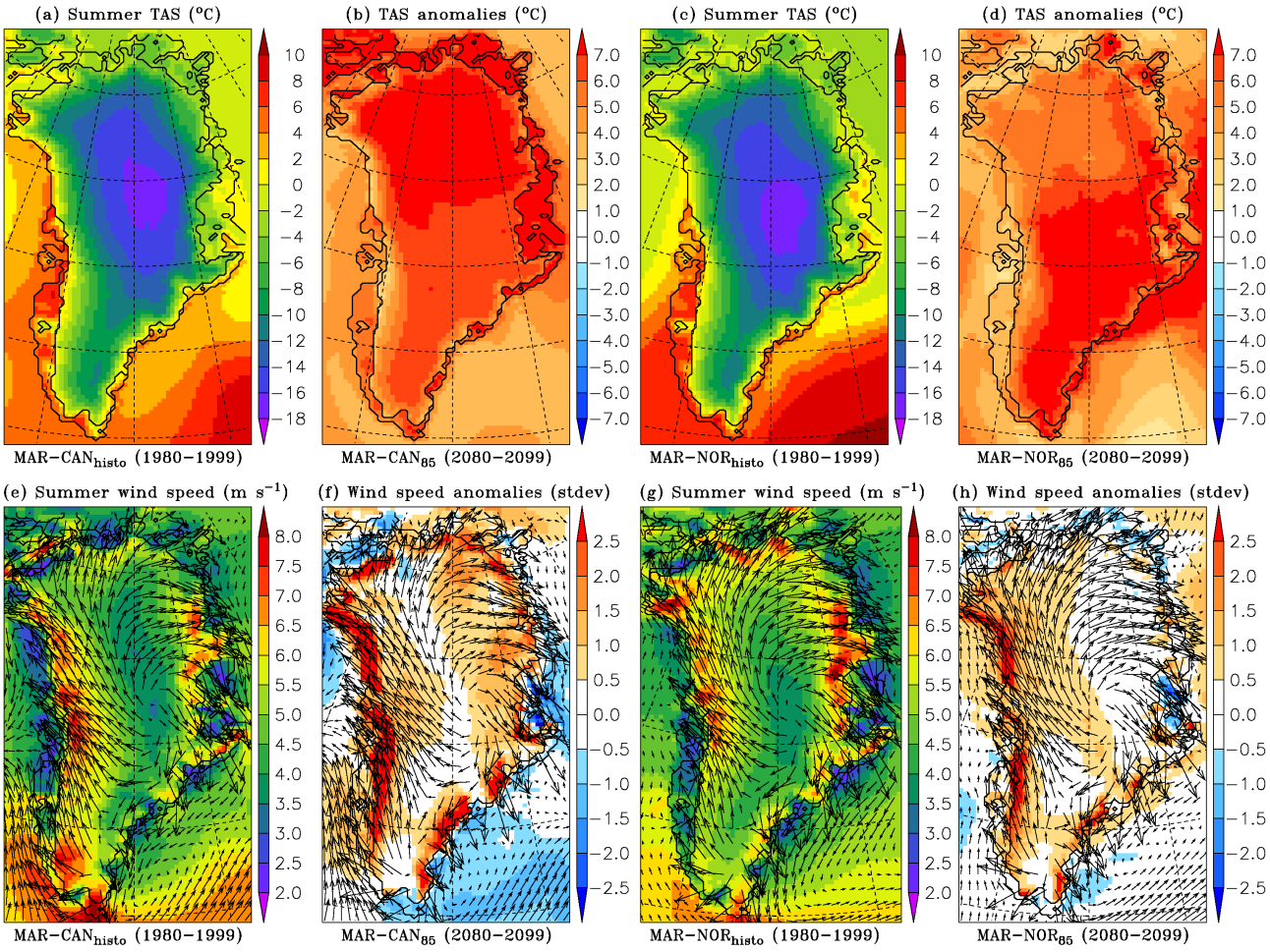

Fig. S5. (a) Summer (June-July-August) near-surface air temperature (°C) from the MAR-CAN$_{histo}$ run over the 1980-1999 period. **(b)** Summer anomalies (°C) of the MAR-CAN$_{85}$ near-surface air temperature compared to **(a)**. **(c)** The same as **(a)**, but for the MAR-NOR$_{histo}$ near-surface air temperature. **(d)** The same as **(b)**, but for the MAR-NOR$_{85}$ anomalies to **(c)**. **(e)** Summer wind speed (m s^{-1}) simulated by MAR-CAN$_{histo}$ over 1980-1999, with average wind direction as vectors. **(f)** Summer anomalies (in standard deviation) of the MAR-CAN$_{85}$ wind speed compared to **(e)**. **(g)** The same as **(a)**, but for the MAR-NOR$_{histo}$ wind speed. **(h)** The same as **(f)**, but for the MAR-NOR$_{85}$ anomalies to **(g)**.

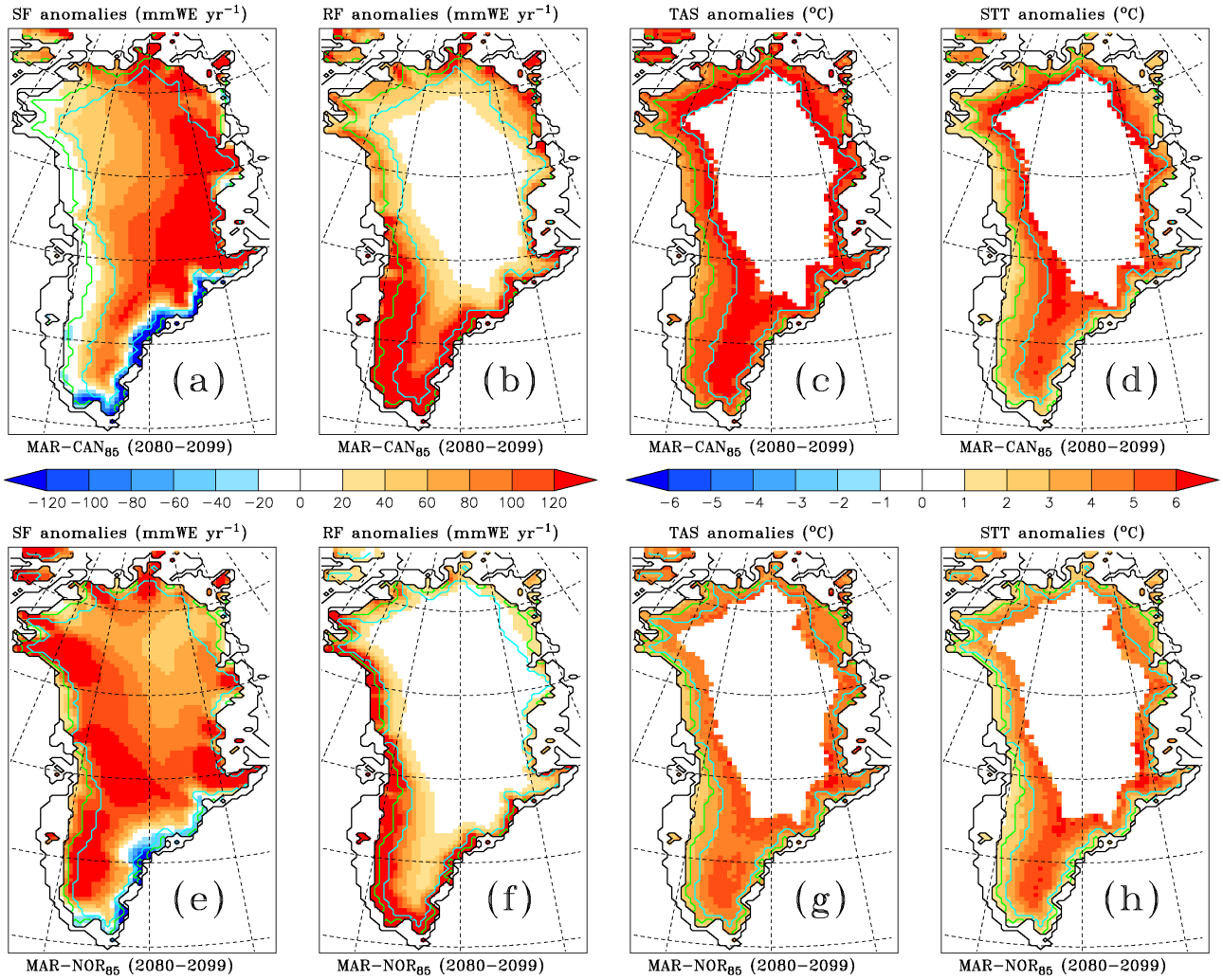

Fig. S6. (a) Summer (June-July-August) snowfall (SF) anomalies (mmWE yr^{-1}) of the 2080-2099 MAR-CAN$_{85}$ simulation over the GrIS, compared to the 1980-1999 MAR-CAN$_{histo}$ simulation. The equilibrium line altitude (ELA) of the 1980-1999 MAR-CAN$_{histo}$ and 2080-2099 MAR-CAN$_{85}$ simulations are drawn in solid green line and solid blue line, respectively. **(b)** The same as **(a)**, but for the summer rainfall (RF) anomalies (mmWE yr^{-1}). **(c)** The same as **(a)**, but for the summer near-surface air temperature (TAS) anomalies (°C) on MSK$_{melt}$. **(d)** The same as **(a)**, but for the summer surface temperature (STT) anomalies (°C) on MSK$_{melt}$. **(e-h)** The same as **(a-d)**, but for the 2080-2099 MAR-NOR$_{85}$ anomalies to 1980-1999 MAR-NOR$_{histo}$.

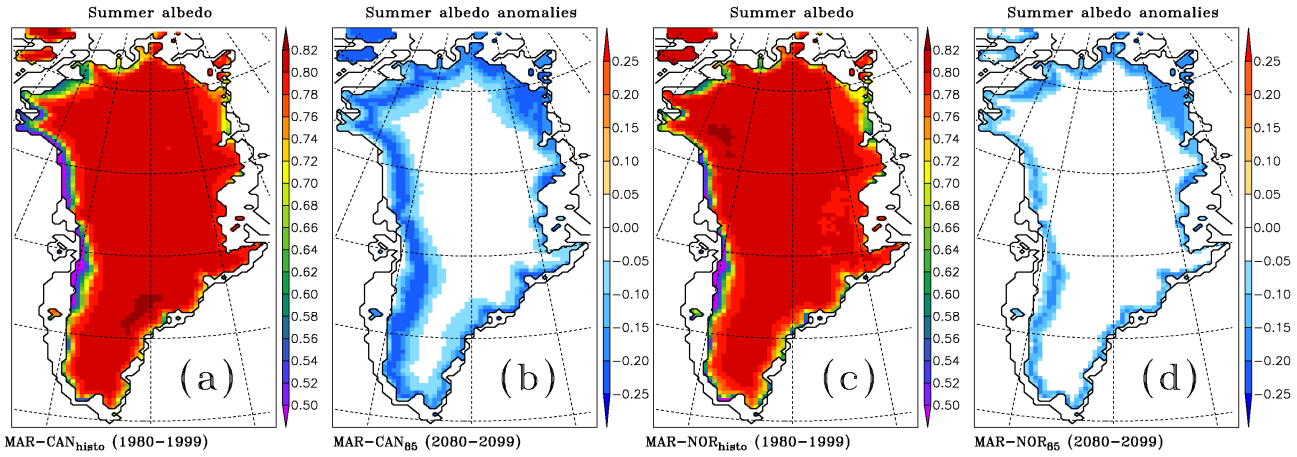

Fig. S7. (a) Summer (June-July-August) surface albedo of the 1980-1999 MAR-CAN$_{histo}$ simulation over the GrIS. **(b)** Summer surface albedo anomalies of the 2080-2099 MAR-CAN$_{85}$ simulation compared to **(a)**. **(c)** The same as **(a)**, but for the 1980-1999 MAR-NOR$_{histo}$ simulation. **(d)** Summer surface albedo anomalies of the 2080-2099 MAR-NOR$_{85}$ simulation compared to **(c)**.

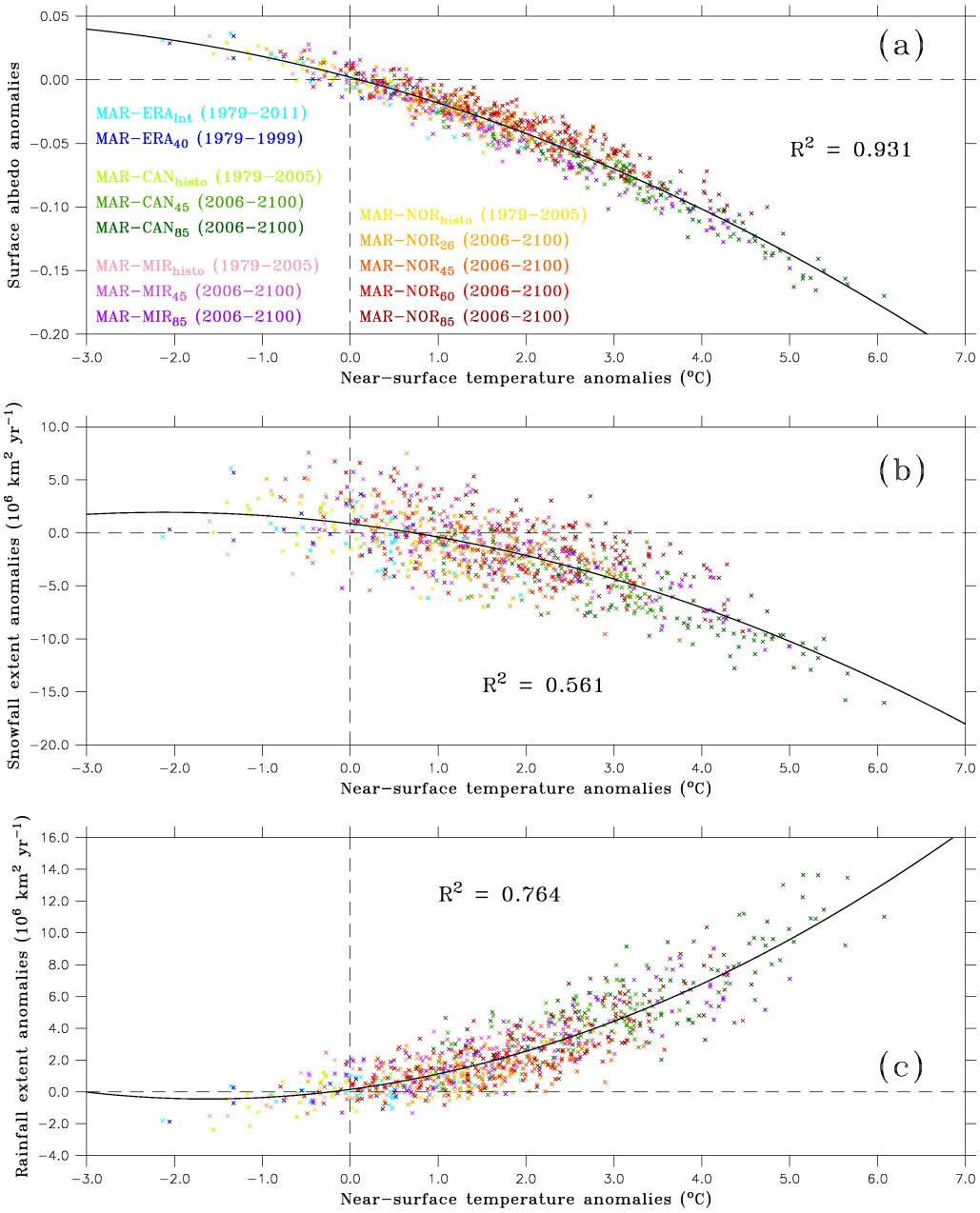

Fig. S8. (a) Surface albedo anomalies according to the near-surface air temperature anomalies (°C) over MSK_{melt}, for the MAR simulations forced by the reanalyses the CMIP5 GCMs, with regression drawn in sold black line. All the anomalies are related to the 1980-1999 average outputs provided by MAR forced with the same forcing fields. **(b)** The same as **(a)**, but for the anomalies of cumulated daily snowfall extents (10^6 km^2 yr^{-1}) on MSK_{melt}, based on significant snowfall higher than 1 mmWE day^{-1}. **(c)** The same as **(b)**, but for the anomalies of cumulated daily rainfall extents (10^6 km^2 yr^{-1}) on MSK_{melt}, based on significant rainfall higher than 1 mmWE day^{-1}.